Solar Physics (2024) 299:30
https://doi.org/10.1007/s11207-024-02272-4

RESEARCH

Multiwavelength Observations of Quasiperiodic Pulsations in the Impulsive Phase of an Eruptive Flare with the *Hard X-Ray Imager* On Board ASO-S and Other Instruments

Fanpeng Shi[1,2] · Dong Li[1,2] · Zongjun Ning[1,2] · Alexander Warmuth[3] · Wei Chen[1,2] · Yang Su[1,2] · Ying Li[1,2] · Jun Xu[1,2] · Yuxiang Song[1,2] · Yuzhi Yang[1,2]

Received: 10 December 2023 / Accepted: 8 February 2024 / Published online: 12 March 2024

Abstract
We investigated the quasiperiodic pulsations (QPPs) of the X1.2 solar flare (SOL2023-01-06T00:57) based on multi-instrument observations, especially the *Hard X-ray Imager* (HXI) on board the *Advanced Space-based Solar Observatory* (ASO-S). The quasiperiod of ≈ 27 s was identified in hard X-rays (HXR) and microwaves using the Markov Chain Monte Carlo method, while no corresponding oscillation was found in soft X-rays. The HXI imaging demonstrates that HXR pulsations arise from the double-footpoint HXR sources. Moreover, the fluctuation of ≈ 27 s period was also present in the nonthermal electron power-law index derived from the X-ray spectra, which is the signature of periodic electron acceleration/precipitation during the impulsive phase. The electron spectral indices not only exhibited the well-known "soft–hard–soft" evolution, but also showed the negative correlation with the HXR pulsations. These results suggest that QPPs directly originate from quasiperiodic injections of accelerated electrons into flare-loop footpoints. We also discuss the possible generation mechanisms for QPPs.

Keywords Oscillations · Solar · Flares · Impulsive phase · X-ray bursts · Association with flares · Radio emission

1. Introduction

Quasiperiodic pulsations (QPPs), the fluctuation of electromagnetic emissions (light curves), are common phenomena in solar and stellar flares. The statistical study of solar flares QPPs

✉ F. Shi
shifp@pmo.ac.cn

Y. Su
yang.su@pmo.ac.cn

1 Key Laboratory of Dark Matter and Space Science, Purple Mountain Observatory, Chinese Academy of Sciences, Nanjing 210023, China

2 School of Astronomy and Space Science, University of Science and Technology of China, Hefei 230026, China

3 Leibniz-Institut für Astrophysik Potsdam (AIP), An der Sternwarte 16, 14482 Potsdam, Germany

clearly demonstrates that QPPs are present in many flares (Simões, Hudson, and Fletcher, 2015; Inglis et al., 2016; Pugh, Broomhall, and Nakariakov, 2017; Dominique et al., 2018; Hayes et al., 2020). QPPs are observed across the entire electromagnetic spectrum, with characteristic periods ranging from subseconds to several minutes (Nakariakov and Melnikov, 2009; Van Doorsselaere, Kupriyanova, and Yuan, 2016; McLaughlin et al., 2018; Kupriyanova et al., 2020; Zimovets et al., 2021).

Many mechanisms have been proposed to explain the observations for QPPs. In general, two main categories can be found, i.e. the modulation by magnetohydrodynamic (MHD) waves in coronal magnetic loops and quasiperiodic magnetic reconnection. In the interpretations by MHD waves, the emissions are modulated by eigenmodes of flare-loop oscillations, in which the sausage (Melnikov et al., 2005; Tian et al., 2016; Li et al., 2020), kink (Kolotkov et al., 2015; Yuan and Van Doorsselaere, 2016a,b; Li et al., 2018; Nakariakov et al., 2021), and slow modes (Wang et al., 2003; Reznikova and Shibasaki, 2011; Wang et al., 2021) may all be candidates for generating QPPs. In the scenario of quasiperiodic magnetic reconnection, charged particles are accelerated periodically to produce enhanced emissions. The reconnection processes could be spontaneous (McLaughlin, Thurgood, and MacTaggart, 2012; Thurgood, Pontin, and McLaughlin, 2017, 2019; Karampelas et al., 2022) or periodically triggered by external waves (Nakariakov et al., 2006; Chen and Priest, 2006; Inglis and Nakariakov, 2009; Li et al., 2022).

The imaging observation of QPPs allows us to analyze the spatial locations of pulsations, which is crucial for understanding the nature of QPPs. With the HXR imaging analysis, it was found that pulsations may originate from flare-loop tops or footpoints, or both of them (Asai et al., 2001; Li and Gan, 2008; Huang et al., 2016; Yuan et al., 2019; Clarke et al., 2021; Li and Chen, 2022). Additionally, the microwave imaging also reveals important information about QPP sources, such as the flare loop and footpoints (Melnikov et al., 2005; Kupriyanova et al., 2010; Reznikova and Shibasaki, 2011; Zimovets, Kuznetsov, and Struminsky, 2013; Kolotkov et al., 2015; Huang et al., 2016) and even the reconnection current sheet (Kou et al., 2022).

In this article, we analyzed the QPPs in an X1.2 flare (SOL2023-01-06T00:57) using multiwavelength observations, including extreme ultraviolet (EUV), white-light, soft X-rays (SXR), hard X-rays (HXR), and microwaves. Based on the HXR imaging and X-ray spectral analysis, the evidence of periodic electron acceleration/precipitation was obtained. Section 2 presents the observations and instruments, followed by the data analysis in Section 3. The discussion and conclusion are shown in Section 4.

2. Observations and Instruments

An X1.2 solar flare (SOL2023-01-06T00:57) occurred in active region NOAA 13182 (S20 E81) located near the eastern limb of the solar disk. According to SXR fluxes recorded by the *X-ray Sensors* (XRS) on board the *Geostationary Operational Environmental Satellite* (GOES), it started at 00:43, peaked at around 00:57, and ended at 01:07 UT. This event was well detected by several instruments, as shown in Table 1, including the *Atmospheric Imaging Assembly* (AIA; Lemen et al., 2012) on board the *Solar Dynamics Observatory* (SDO; Pesnell, Thompson, and Chamberlin, 2012), the *Hard X-ray Imager* (HXI; Su et al., 2019; Zhang et al., 2019), the *White-light Solar Telescope* (WST) of the *Lyman-alpha (Lyα) Solar Telescope* (LST; Li et al., 2019) on board the *Advanced Space-based Solar Observatory* (ASO-S; Gan et al., 2019, 2023), the *Spectrometer/Telescope for Imaging X-rays* (STIX; Krucker et al., 2020) on board the *Solar Orbiter* (SolO; Müller et al., 2020), the

Table 1 Observational instruments and data used in this study.

Instrument	Wavelength	Cadence (s)	Pixel size (arcsec)	Description	Dimension
GOES/XRS	1 – 8 Å	≈ 1	–	SXR	1D
SDO/AIA	94, 131 Å	12	0.6	EUV imaging	2D
	1600 Å	24	0.6	UV imaging	2D
ASO-S/HXI	15 – 25, 25 – 50, 50 – 84 keV	0.5	–	HXR/SXR	1D
	15 – 20, 25 – 50, 50 – 84 keV	–	2	Imaging	2D
	10 – 300 keV	4	–	Spectra	1D
ASO-S/LST/WST	360 nm	120	0.5	White-light imaging	2D
SolO/STIX	15 – 25, 25 – 50, 50 – 84 keV	0.5	–	HXR/SXR	1D
	4 – 150 keV	4	–	Spectra	1D
Fermi/GBM	50 – 101 keV	1	–	HXR	1D
KW	20 – 80 keV	0.5	–	HXR	1D
NoRP	17, 35 GHz	1	–	Microwave	1D
CBS	35.25 – 39.25 GHz	≈ 0.53	–	Microwave	1D

Fermi Gamma-ray Burst Monitor (GBM; Meegan et al., 2009), the *Konus-Wind* (KW; Lysenko et al., 2022), the *Nobeyama Radio Polarimeters* (NoRP; Nakajima et al., 1985), and the *Chashan Broadband Solar millimeter spectrometer* (CBS; Shang et al., 2022, 2023; Yan et al., 2023; note that it is the first solar-dedicated radio spectrometer in the millimeter regime).

ASO-S/HXI has a higher temporal cadence in the burst mode and hence the light curves were interpolated to the uniform 0.5 s in this study. Likewise, the time series of Fermi/GBM and KW were interpolated to lower cadences of 1 s and 0.5 s, respectively.

In contrast to these near-Earth assets, SolO/STIX was at a distance of 0.95 AU from the Sun, and its position with respect to solar longitude was ≈ 23.6° east from the Sun–Earth line at the time of the event.

Figures 1a–c show the AIA 94 Å, 131 Å, and 1600 Å images taken at the impulsive phase of the flare. The AIA 94 Å and 131 Å passbands reflect the flaring plasma with the characteristic temperature of ≈ 6 MK and ≈ 10 MK, respectively. The AIA 1600 Å flare excess emission is of chromospheric origin (Simões et al., 2019). From the AIA movie (aia94_movie.mp4), we can see the underlying bright compact "postflare" loops accompanied by the overlying large-scale eruption and the fall of matter. This event was a double-ribbon flare, the two ribbons were connected by flare loops with the prominent cusp structure above the loops. Furthermore, the contours of HXI images of three energy bands are overlaid, the contour levels represent 25%, 50%, and 75% of the peak intensity. At the beginning of the eruption (panel a), the 25 – 50 keV band (cyan) shows double HXR sources, while the 50 – 84 keV (magenta) shows a single source. Subsequently, both 25 – 50 keV and 50 – 84 keV bands show double sources, which coincide with the footpoints of EUV compact loops. The lower energy band 15 – 20 keV (red) exhibits some ejected structures, as well as the footpoints and loop structures. The HXR images are reconstructed by the HXI Clean method (HXI pattern-based Clean algorithm) using the detectors from D19 to D91, since the fine grids (i.e. D1 – D18) still need to be carefully calibrated. Figure 1d illustrates that the white-light brightening shows the same location as the HXR sources. This flare has also been confirmed as a white-light flare by Jing et al. (2024).

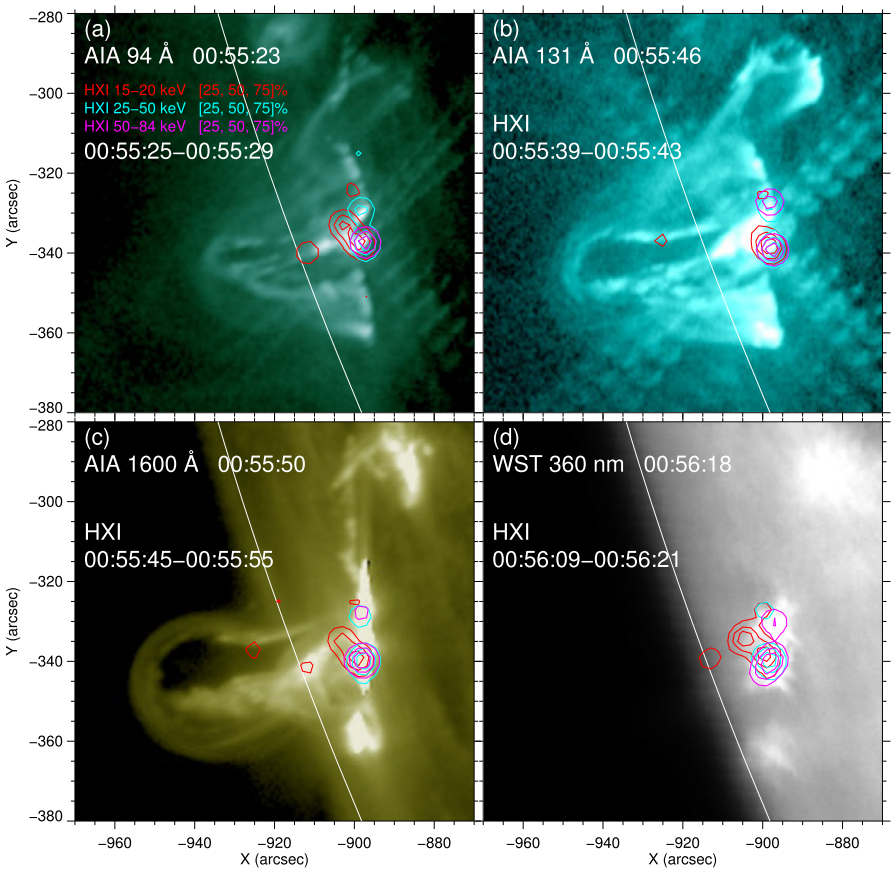

Figure 1 (**a**) AIA 94 Å, (**b**) 131 Å, and (**c**) 1600 Å images taken during the impulsive phase of the flare. The HXR contours of three energy bands are overlaid. The contour levels are 25%, 50%, and 75% of the peak intensity. (**d**) LST/WST 360 nm white-light image with overplotted HXR contours.

3. Data Analysis

3.1. The Identification of QPPs

QPPs were identified as intensity fluctuations above the noise level. In this study, the Markov Chain Monte Carlo (MCMC) method was used to recognize the oscillatory signals. The details of the MCMC method for detecting periodic signals can be seen in previous literature (Vaughan, 2005, 2010; Inglis, Ireland, and Dominique, 2015; Inglis et al., 2016; Hayes et al., 2019, 2020; Liang et al., 2020; Guo et al., 2023; Shi et al., 2023). This method fits the Fourier power spectral density (PSD) of a time series with a model and determines the best-fit parameters. We selected the three-parameter model, which is a power-law plus a constant, i.e. $M = Af^{-\alpha} + C$, where f is the Fourier frequency, $Af^{-\alpha}$ and C reflect the properties of red and white noise in Fourier PSD, respectively.

Figure 2 plots the time series and their MCMC simulation results for multiwavelengths, including the HXI 50 – 84 keV (panel a), 25 – 50 keV (panel c), 15 – 25 keV (panel e), STIX 50 – 84 keV (panel b), 25 – 50 keV (panel d), 15 – 25 keV (panel f),

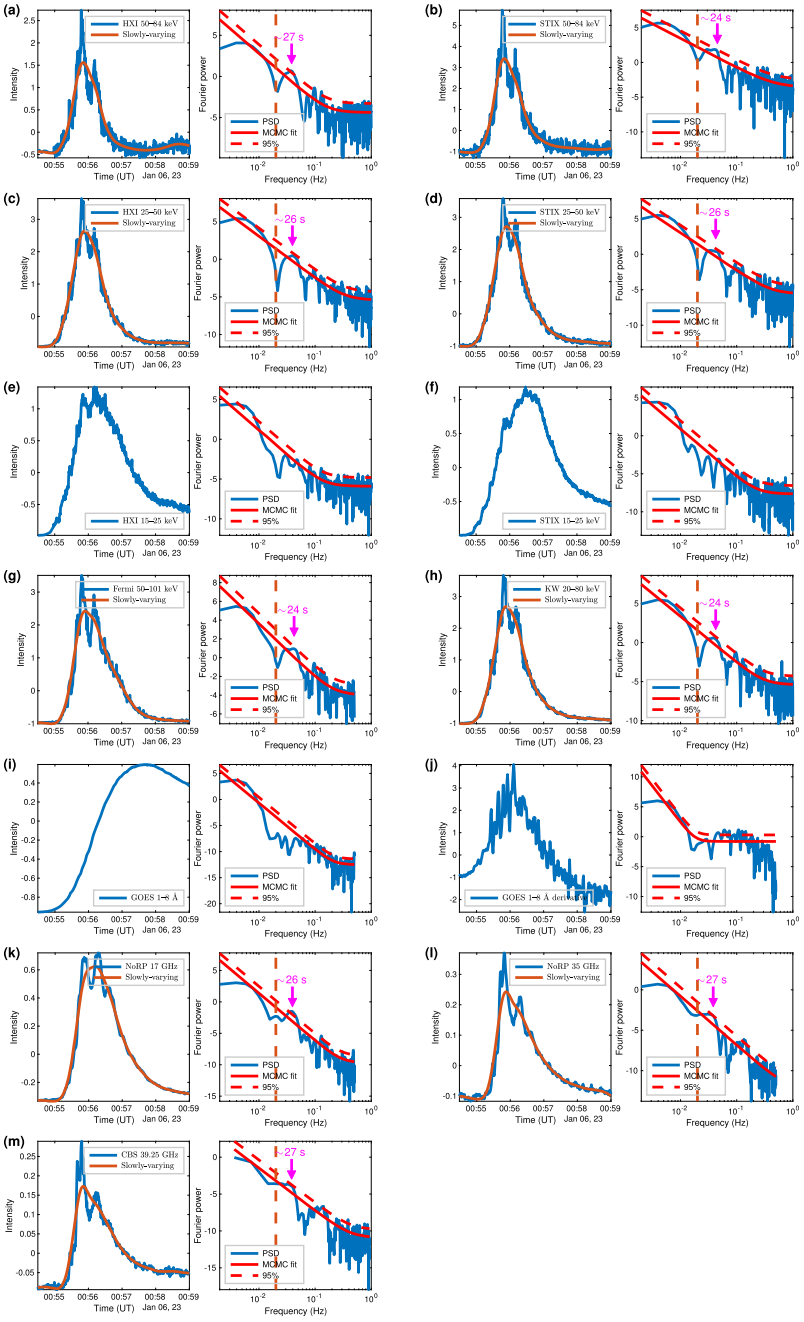

Figure 2 (**a**) The HXI 50 – 84 keV intensity (blue) and its slowly varying components (orange) in the left panel. The Fourier PSD (blue), best-fit (red solid), and the 95% confidence level (red dashed) in the right panel. The vertical orange line represents the cutoff threshold between rapidly (high-) and slowly varying (low-frequency) components. The prominent peak of ≈ 27 s is also marked. (**b**)–(**m**) Similar to (**a**), results for other instruments and wavelengths. For the (**e**)–(**f**) and (**i**)–(**j**), slowly varying components were not plotted because the ≈ 27 s QPPs are not detected in these wavelengths.

Fermi 50 – 101 keV (panel g), KW 20 – 80 keV (panel h), GOES 1 – 8 Å (panel i), 1 – 8 Å derivative (panel j), NoRP 17 GHz (panel k), NoRP 35 GHz (panel l), and the CBS 39.25 GHz (panel m). As shown in Figure 2a, the intensity (blue) and its slowly varying components (orange) are plotted in the left panel, while the Fourier PSD (blue), best-fit (red solid), and the 95% confidence level (red dashed) are plotted in the right panel (periodogram). The PSD at the position of ≈ 27 s shows a prominent peak above the 95% confidence level, indicating that the period of QPPs in HXI 50 – 84 keV is about 27 s. Figure 2c shows a similar peak of ≈ 26 s in HXI 25 – 50 keV, but it seems to have just reached the 95% confidence level. Likewise, STIX 50 – 84 keV (≈ 24 s), STIX 50 – 84 keV (≈ 26 s), Fermi 50 – 101 keV (≈ 24 s), Fermi 50 – 101 keV (≈ 24 s), KW 20 – 80 keV (≈ 24 s), NoRP 35 GHz (≈ 27 s), and CBS 39.25 GHz (≈ 27 s) all appear to have just reached the 95% confidence level, while NoRP 17 GHz (≈ 26 s) shows a peak above that. However, GOES 1 – 8 Å and its derivative (an approximation for the HXR), HXI 15 – 25 keV, and STIX 15 – 25 keV, do not show any definite periodic signals above the red-noise level, which suggests that the absence of ≈ 27 s QPPs in SXR and HXR below 25 keV. Therefore, our observation confirms the existence of ≈ 27 s QPPs in HXR above 25 keV and microwaves.

The presence of a period of about 27 s is convincingly shown. It is also notable that the PSD in Figure 2 show peaks with a frequency of about ≈ 10 s, near the 95% confidence level above the red-noise level, which may be another quasiperiodic signal. Additionally, as shown in the GOES 1 – 8 Å derivative curve, there are some clear pulsations with a period of ≈ 10 s. Although these oscillations are higher than the random white noise in Fourier space, rather than the red noise, they are indeed likely to be the ≈ 10 s QPPs signals.

3.2. QPPs in Nonthermal Emissions

After identifying the ≈ 27 s QPPs, it is natural to decompose the light curves into rapidly and slowly varying components via the fast Fourier transform (FFT) method. A value of 50 s (0.02 Hz) was adopted as the cutoff threshold between rapidly (high-) and slowly varying (low-frequency) components, as marked by the vertical orange line in the periodogram in Figure 2. Figure 3a plots the self-normalized light curves between 00:54 and 00:59 UT, including the GOES 1 – 8 Å (purple), HXI 15 – 25 keV (dark blue), 25 – 50 keV (black), 50 – 84 keV (blue), STIX 15 – 25 keV (orange), 25 – 50 keV (red), 50 – 84 keV (green), Fermi 50 – 101 keV (gold), and the KW 20 – 80 keV (pink). Figure 3b plots the CBS spectrum with the microwave light curves (NoRP 17 GHz, 35 GHz, and CBS 39.25 GHz) overplotted. The HXRs exhibit similar pulsations as the microwaves during the impulsive phase, i.e. 00:55 – 00:57 UT, as marked by the gray background. Figure 3c shows the corresponding rapidly varying components that are obtained from the FFT method mentioned above. Morlet-wavelet analysis was performed on the rapidly varying components to determine the periodicity. This routine was provided by Torrence and Compo (1998). Figure 3d plots the wavelet power spectra of the detrended HXI 50 – 84 keV emission, and the 95% significance level is marked. The significant period of ≈ 27 s is found in the global power spectrum, which is consistent with the periodicity found in the MCMC simulation. As for the ≈ 10 s signal mentioned before, the corresponding weak signatures are also visible on the wavelet spectrum, almost simultaneously with the ≈ 27 s oscillation, which could be the sign of second or third harmonics.

Both the HXR and microwave emissions here are caused by nonthermal electrons – by nonthermal bremsstrahlung for HXR, and gyrosynchrotron emission for microwaves. Figure 4 gives the crosscorrelation diagrams between the rapidly varying components of HXI

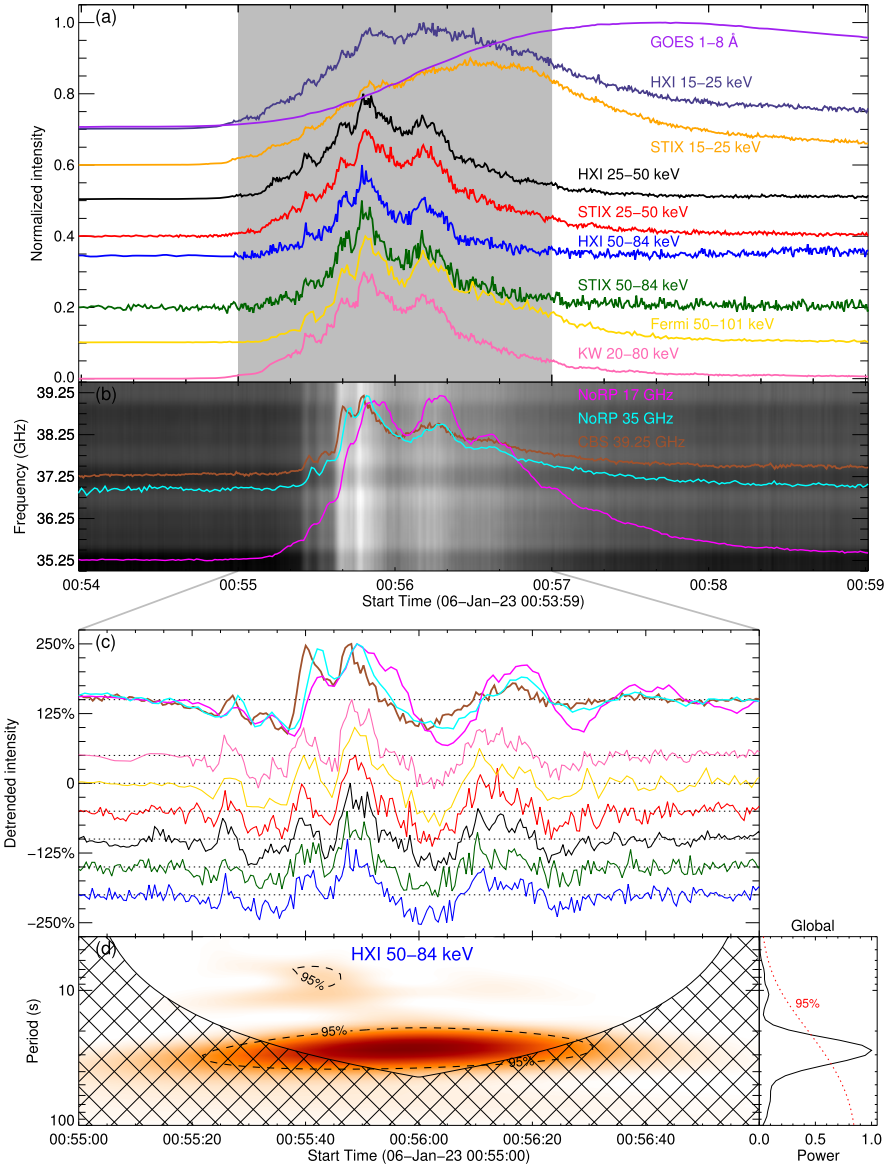

Figure 3 (**a**) The self-normalized light curves between 00:54 and 00:59 UT, including the GOES 1 – 8 Å (purple), HXI 15 – 25 keV (dark blue), 25 – 50 keV (black), 50 – 84 keV (blue), STIX 15 – 25 keV (orange), 25 – 50 keV (red), 50 – 84 keV (green), Fermi 50 – 101 keV (gold), and the KW 20 – 80 keV (pink). (**b**) The CBS spectrum with the microwave light curves (NoRP 17 GHz, 35 GHz, and CBS 39.25 GHz) are overplotted. (**c**) The rapidly varying components of light curves at 00:55 – 00:57 UT. (**d**) The Morlet-wavelet spectra of the detrended HXI 50 – 84 keV emission. The 95% significance level is also marked.

50 – 84 keV and that of other wavelengths at 00:55 – 00:57 UT. Their correlation coefficients (CCs) are also labeled. The HXI 50 – 84 keV data are interpolated to the same temporal resolution as Fermi, NoRP, and CBS. These diagrams show good positive correlation, with the

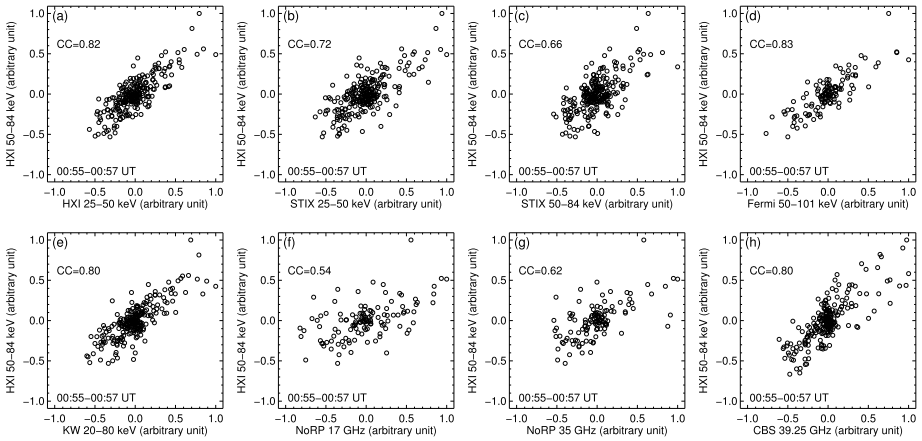

Figure 4 The intensity fluctuations at HXI 50 – 84 keV vs. at (**a**) HXI 25 – 50 keV, (**b**) STIX 25 – 50 keV, (**c**) STIX 50 – 84 keV, (**d**) Fermi 50 – 101 keV, (**e**) KW 20 – 80 keV, (**f**) NoRP 17 GHz, (**g**) NoRP 35 GHz, and (**h**) CBS 39.25 GHz at 00:55 – 00:57 UT. The correlation coefficient (CC) is also added.

CCs all larger than 0.54 and the maximum as high as 0.83, which is sufficient to illustrate the almost inphase oscillations between HXRs and microwaves.

3.3. QPPs of Nonthermal Electron Spectral Index

We also performed X-ray spectral analysis on the HXI and STIX data during the impulsive phase (i.e. 00:55 – 00:57 UT) using the Object Spectral Analysis Executive (OSPEX) software package within the Solar SoftWare (SSW). These spectra were obtained over time intervals of 4 s and fitted by single-temperature thermal bremsstrahlung (vth) plus a nonthermal thick-target single power-law (thick2_vnorm) model. These fits also included the isotropic albedo correction (Kontar et al., 2006), i.e. the actual fit model was "vth+thick2_vnorm+albedo". Figure 5 shows four examples of fitting results around the time of the HXR peak, in which panels a and b show the HXI spectral fitting, and panels c and d show the STIX result. The black profiles are the background-subtracted spectral data with error bars, and the fitting thermal (blue) and nonthermal components (green) are overplotted. The reduced residuals are shown at the bottom of the spectra, which represent the deviation between the spectral data (black) and total fitting (red). The vertical red lines indicate the upper and lower limits of energy bands for fitting. The derived physical parameters are also given.

In terms of thermal parameters, the differences in plasma temperature (T) between HXI and STIX were not significant, with values of ≈ 19 MK and ≈ 21 MK, respectively, but there were minor differences in the emission measure (EM). The EM was approximately $(3.96-4.42) \times 10^{49}$ cm^{-3} for HXI, while it was $(0.73-0.90) \times 10^{49}$ cm^{-3} for STIX during the same time interval. This discrepancy in the thermal component is most likely due to the fact that the STIX spectral fits go down to 4 keV and also have a higher energy resolution at low energies as compared to HXI, for which 12 keV was used as the minimum energy. In contrast, the fitted nonthermal parameters showed a very good agreement. The electron fluxes for HXI and STIX were estimated to be $(5.11-5.95)$ and $(4.90-5.72) \times 10^{33}$ s^{-1} keV^{-1}. Additionally, the nonthermal electron spectral indices (δ)

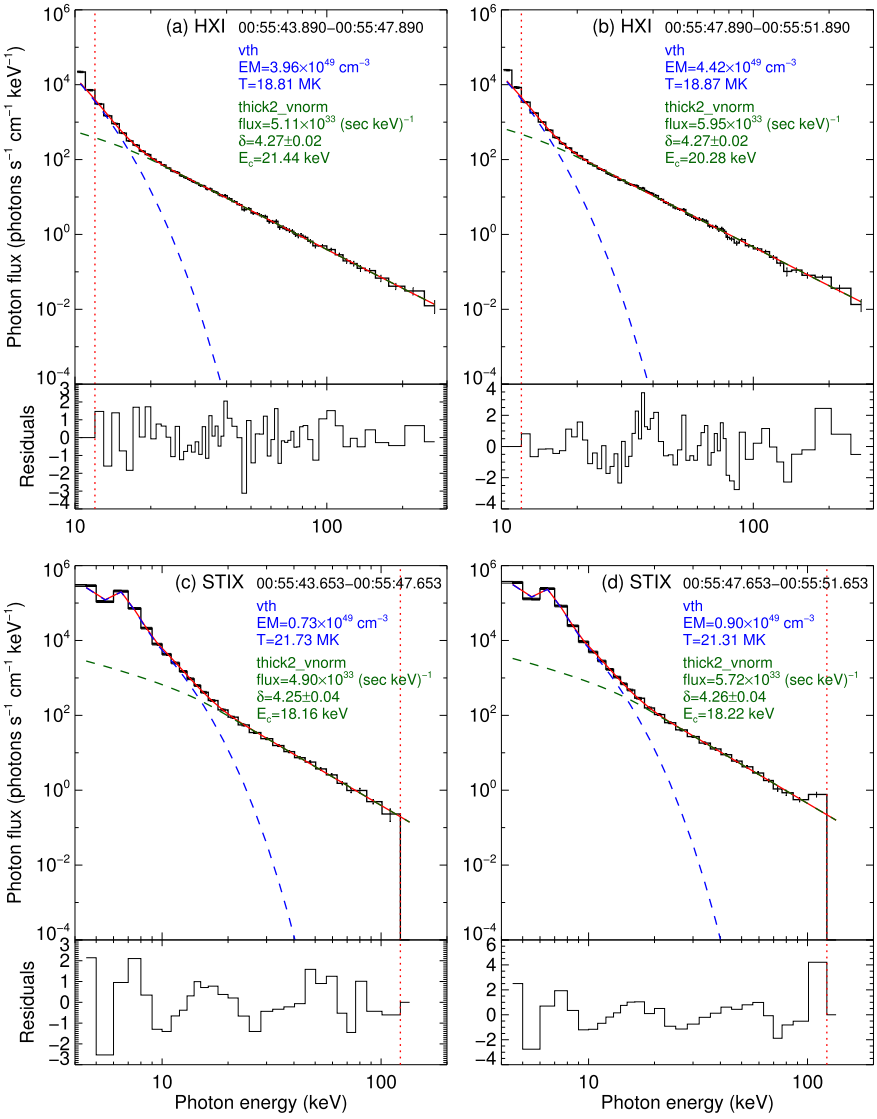

Figure 5 (**a**) and (**b**) HXI spectra and fitting results with the "vth+thick2_vnorm+albedo" model. Shown is the background-subtracted spectral data (black) with error bars, the thermal (blue) and nonthermal fitting components (green), and the total fit (red). The reduced residuals are shown at the bottom of the spectra. The vertical red lines indicate the lower limit of the energy range used for fitting. The fitting parameters are also given. (**c**) and (**d**) Similar to (**a**) and (**b**), for the STIX spectra and fitting results.

were almost the same considering the sigma (σ) error, and the low-energy cutoffs (E_c) of HXI ($\approx$20 keV) were only marginally larger than that of STIX ($\approx$18 keV).

Figure 6a shows the temporal evolution of nonthermal electron spectral indices (red for HXI, blue for STIX) from 00:55 to 00:57 UT, with the light curve of HXI 50 – 84 keV overplotted. The spectral indices of HXI and STIX not only show the well-known "soft–hard–soft" trend (Benz, 1977; Brown and Loran, 1985; Lin and Schwartz, 1987; Fletcher

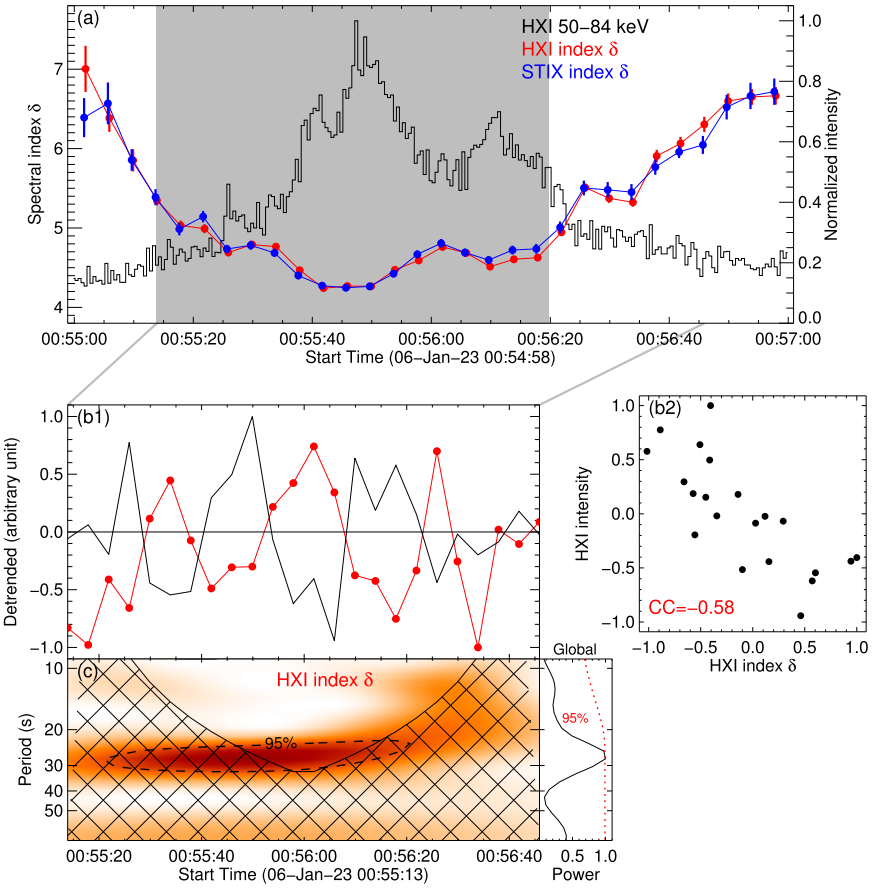

Figure 6 (**a**) The temporal evolution of nonthermal electron spectral indices (red for HXI, blue for STIX) from 00:55 to 00:57 UT, and the normalized intensity of HXI 50 – 84 keV. (**b1**) and (**b2**) The correlation between the detrended spectral index and the detrended HXR intensity. (**c**) The Morlet-wavelet spectra of the detrended spectral index. The 95% significance level is also marked.

and Hudson, 2002; Grigis and Benz, 2004), but also show the negative correlation with the HXR emission. In order to investigate this correlation, Figure 6b1 plots the detrended HXI spectral index and the detrended HXR intensity, which were derived with the same FFT method as above. To compare with the spectral index, the detrended HXR intensity had been interpolated to the temporal resolution of 4 s. Figure 6b2 plots the correlation between the detrended spectral index and HXR intensity. Although panel b2 exhibits a good negative correlation, the CC is only -0.58, which could be caused by the calculation using only 24 points. We also performed the wavelet analysis on the detrended spectral index, as shown in Figure 6c. The Morlet-wavelet spectra show a peak at ≈ 27 s, reaching the 95% significance level, which is consistent with the period of QPPs analyzed before. The same dominant period implies the origin of QPPs, i.e. the periodic electron acceleration/precipitation during the impulsive phase.

4. Discussion and Conclusion

We studied the QPPs of the X1.2 solar flare (SOL2023-01-06T00:57) based on multi-instrument observations. The ≈ 27 s QPPs were identified in HXRs and microwaves during the impulsive phase, but not found in the SXR thermal emission. The weak signatures of another quasiperiod of ≈ 10 s were also present, which may be the sign of second or third harmonics. Spatial analysis of HXI imaging demonstrates that HXR pulsations originate from the double-footpoint HXR sources. Furthermore, the nonthermal electron spectral indices also show the ≈ 27 s oscillation via the X-ray spectral analysis using HXI and STIX data. Our results support the scenario of quasiperiodic injections of accelerated electrons, in which periodic electrons spiral along magnetic field lines in flare loops to generate microwaves, and then precipitate into the chromosphere at the double footpoints to produce HXR emissions.

Figure 1 indicates that there are remote hook-like flare ribbons and in general the development of this flare resembles a picture of the three-dimensional (3D) standard flare model (e.g. Janvier et al., 2014). Although after around 01:05 UT, well after the end of QPPs, the eruption observed in EUV stopped, i.e. the flare was accompanied by a confined eruption and a coronal mass ejection was not observed in white light in this event. In this scenario, a slipping reconnection may occur in the current layer, which may be accompanied by a displacement of HXR sources along the magnetic polarity-inversion line. There are observations indicating that such magnetic reconnection can occur in a quasiperiodic mode in some flares (Li and Zhang, 2015; Li et al., 2016). A simulation work performed by Thurgood, Pontin, and McLaughlin (2017) demonstrated that reconnection at 3D magnetic null points can proceed naturally in a time-dependent and periodic fashion, illustrating that oscillatory reconnection likely plays a role in the observed QPPs.

QPPs accompanied by motions of HXR sources along a polarity-inversion line can be also interpreted in terms of quasiperiodic triggering or modulation of magnetic reconnection in a current sheet by slow magnetoacoustic waves (Nakariakov and Zimovets, 2011) or by flapping oscillations (Artemyev and Zimovets, 2012). However, due to the observation perspective of this flare arcade, or due to limited angular resolution of the used HXI collimating grids, motion of HXR sources was hard to observe in this event. This does not allow us to conclude which of these mechanisms is the more probable as the origin of QPPs.

There are other theoretical works (models) showing the possibility of quasiperiodic modulation of physical parameters in the cusp region, the signs of which are observed in this flare. Takasao and Shibata (2016) revealed the above-the-loop-top oscillation controlled by the backflow of the reconnection outflow, which then excited quasiperiodic propagating fast-mode magnetoacoustic waves (QPFs), a model known as a "magnetic tuning fork". They also found that the above-the-loop-top region presented shocks and waves, as well as the periodic variation of the termination-shock strength. The termination shock is a promising driver for particle acceleration in flares (Chen et al., 2015). This means that electrons could be accelerated periodically through this physical process located at the above-the-loop-top region.

QPPs with short periods were generally interpreted as sausage modes in terms of MHD waves (Nakariakov, Melnikov, and Reznikova, 2003; Melnikov et al., 2005; Inglis, Nakariakov, and Melnikov, 2008; Van Doorsselaere et al., 2011; Kolotkov et al., 2015). Tian et al. (2016) found strong evidence for trapped sausage modes, which explained the ≈ 25 s QPPs. However, in this study, due to the explosive and highly dynamic nature of the impulsive phase, the standing MHD waves may not be effectively established in the flare loops.

We report here some of the first observations obtained with new instruments, which show the capabilities to investigate QPPs using the joint observations of HXI and STIX. In the

future, we will apply this to more events to obtain statistically sound results. For example, Collier et al. (2023) found periods across the range of 4 – 128 s in a study of several STIX flares, and the joint observation may help to investigate the causes of the variation of the QPP periods.

Supplementary Information The online version contains supplementary material available at https://doi.org/10.1007/s11207-024-02272-4.

Acknowledgment We thank the referee for valuable comments. ASO-S mission is supported by the Strategic Priority Research Program on Space Science, the Chinese Academy of Sciences, Grant No. XDA15320000. Solar Orbiter is a space mission of international collaboration between ESA and NASA, operated by ESA. We appreciate the teams of GOES, SDO, Fermi, KW, NoRP, and CBS for their open data-use policy.

Author contributions F.S., D.L., and Z.N. wrote the main manuscript text, A.W. and W.C. prepared Figures 5 – 6, Y.S. and Y.L. prepared Figure 1. J.X., Y.S., and Y.Y. participated in the discussion. All authors reviewed the manuscript.

Funding This work is supported by the Strategic Priority Research Program of the Chinese Academy of Sciences, Grant No. XDB0560000. This work is also funded by the National Key R&D Program of China2022YFF0503002 (2022YFF0503000), NSFC under grants 12073081, 12333010, and 11820101002.

Data Availability ASO-S data: http://aso-s.pmo.ac.cn/sodc/dataArchive.jsp. SolO data: https://soar.esac.esa.int/soar/. SDO data: http://jsoc.stanford.edu. KW data: http://www.ioffe.ru/LEA/kwsun/. NoRP data: http://solar.nro.nao.ac.jp/norp/index.html. GOES and Fermi data can be downloaded via SSW. CBS data can be obtained by contacting the instrument team.

Materials Availability The movie (aia94_movie.mp4) of Figure 1 is available.

Declarations

Competing interests The authors declare no competing interests.

References

Artemyev, A., Zimovets, I.: 2012, Stability of current sheets in the solar corona. *Solar Phys.* **277**, 283. DOI. ADS.

Asai, A., Shimojo, M., Isobe, H., Morimoto, T., Yokoyama, T., Shibasaki, K., Nakajima, H.: 2001, Periodic acceleration of electrons in the 1998 November 10 solar flare. *Astrophys. J. Lett.* **562**, L103. DOI. ADS.

Benz, A.O.: 1977, Spectral features in solar hard X-ray and radio events and particle acceleration. *Astrophys. J.* **211**, 270. DOI. ADS.

Brown, J.C., Loran, J.M.: 1985, Possible evidence for stochastic acceleration of electrons in solar hard X-ray bursts observed by SMM. *Mon. Not. Roy. Astron. Soc.* **212**, 245. DOI. ADS.

Chen, P.F., Priest, E.R.: 2006, Transition-region explosive events: reconnection modulated by p-mode waves. *Solar Phys.* **238**, 313. DOI. ADS.

Chen, B., Bastian, T.S., Shen, C., Gary, D.E., Krucker, S., Glesener, L.: 2015, Particle acceleration by a solar flare termination shock. *Science* **350**, 1238. DOI. ADS.

Clarke, B.P., Hayes, L.A., Gallagher, P.T., Maloney, S.A., Carley, E.P.: 2021, Quasi-periodic particle acceleration in a solar flare. *Astrophys. J.* **910**, 123. DOI. ADS.

Collier, H., Hayes, L.A., Battaglia, A.F., Harra, L.K., Krucker, S.: 2023, Characterising fast-time variations in the hard X-ray time profiles of solar flares using Solar Orbiter's STIX. *Astron. Astrophys.* **671**, A79. DOI. ADS.

Dominique, M., Zhukov, A.N., Dolla, L., Inglis, A., Lapenta, G.: 2018, Detection of quasi-periodic pulsations in solar EUV time series. *Solar Phys.* **293**, 61. DOI. ADS.

Fletcher, L., Hudson, H.S.: 2002, Spectral and spatial variations of flare hard X-ray footpoints. *Solar Phys.* **210**, 307. DOI. ADS.

Gan, W.-Q., Zhu, C., Deng, Y.-Y., Li, H., Su, Y., Zhang, H.-Y., Chen, B., Zhang, Z., Wu, J., Deng, L., Huang, Y., Yang, J.-F., Cui, J.-J., Chang, J., Wang, C., Wu, J., Yin, Z.-S., Chen, W., Fang, C., Yan, Y.-H., Lin, J., Xiong, W.-M., Chen, B., Bao, H.-C., Cao, C.-X., Bai, Y.-P., Wang, T., Chen, B.-L., Li, X.-Y., Zhang, Y., Feng, L., Su, J.-T., Li, Y., Chen, W., Li, Y.-P., Su, Y.-N., Wu, H.-Y., Gu, M., Huang, L., Tang, X.-J.: 2019, Advanced Space-based Solar Observatory (ASO-S): an overview. *Res. Astron. Astrophys.* **19**, 156. DOI. ADS.

Gan, W., Zhu, C., Deng, Y., Zhang, Z., Chen, B., Huang, Y., Deng, L., Wu, H., Zhang, H., Li, H., Su, Y., Su, J., Feng, L., Wu, J., Cui, J., Wang, C., Chang, J., Yin, Z., Xiong, W., Chen, B., Yang, J., Li, F., Lin, J., Hou, J., Bai, X., Chen, D., Zhang, Y., Hu, Y., Liang, Y., Wang, J., Song, K., Guo, Q., He, L., Zhang, G., Wang, P., Bao, H., Cao, C., Bai, Y., Chen, B., He, T., Li, X., Zhang, Y., Liao, X., Jiang, H., Li, Y., Su, Y., Lei, S., Chen, W., Li, Y., Zhao, J., Li, J., Ge, Y., Zou, Z., Hu, T., Su, M., Ji, H., Gu, M., Zheng, Y., Xu, D., Wang, X.: 2023, The Advanced Space-Based Solar Observatory (ASO-S). *Solar Phys.* **298**, 68. DOI. ADS.

Grigis, P.C., Benz, A.O.: 2004, The spectral evolution of impulsive solar X-ray flares. *Astron. Astrophys.* **426**, 1093. DOI. ADS.

Guo, Y., Liang, B., Feng, S., Yuan, D., Nakariakov, V.M., Dai, W., Yang, Y.: 2023, Feature identification and statistical characteristics of quasi-periodic pulsation in solar flares using the Markov-chain-Monte-Carlo approach. *Astrophys. J.* **944**, 16. DOI. ADS.

Hayes, L.A., Gallagher, P.T., Dennis, B.R., Ireland, J., Inglis, A., Morosan, D.E.: 2019, Persistent quasi-periodic pulsations during a large X-class solar flare. *Astrophys. J.* **875**, 33. DOI. ADS.

Hayes, L.A., Inglis, A.R., Christe, S., Dennis, B., Gallagher, P.T.: 2020, Statistical study of GOES X-ray quasi-periodic pulsations in solar flares. *Astrophys. J.* **895**, 50. DOI. ADS.

Huang, J., Kontar, E.P., Nakariakov, V.M., Gao, G.: 2016, Quasi-periodic acceleration of electrons in the flare on 2012 July 19. *Astrophys. J.* **831**, 119. DOI. ADS.

Inglis, A.R., Ireland, J., Dominique, M.: 2015, Quasi-periodic pulsations in solar and stellar flares: re-evaluating their nature in the context of power-law flare Fourier spectra. *Astrophys. J.* **798**, 108. DOI. ADS.

Inglis, A.R., Nakariakov, V.M.: 2009, A multi-periodic oscillatory event in a solar flare. *Astron. Astrophys.* **493**, 259. DOI. ADS.

Inglis, A.R., Nakariakov, V.M., Melnikov, V.F.: 2008, Multi-wavelength spatially resolved analysis of quasi-periodic pulsations in a solar flare. *Astron. Astrophys.* **487**, 1147. DOI. ADS.

Inglis, A.R., Ireland, J., Dennis, B.R., Hayes, L., Gallagher, P.: 2016, A large-scale search for evidence of quasi-periodic pulsations in solar flares. *Astrophys. J.* **833**, 284. DOI. ADS.

Janvier, M., Aulanier, G., Bommier, V., Schmieder, B., Démoulin, P., Pariat, E.: 2014, Electric currents in flare ribbons: observations and three-dimensional standard model. *Astrophys. J.* **788**, 60. DOI. ADS.

Jing, Z., Li, Y., Feng, L., Li, H., Huang, Y., Li, Y., Su, Y., Chen, W., Tian, J., Song, D., Li, J., Xue, J., Zhao, J., Lu, L., Ying, B., Zhang, P., Su, Y., Zhang, Q., Li, D., Ge, Y., Li, S., Li, Q., Li, G., Liu, X., Shi, G., Shan, J., Tian, Z., Zhou, Y., Gan, W.: 2024, A statistical study of solar white-light flares observed by the White-Light Solar Telescope of the Lyman-Alpha Solar Telescope on the Advanced Space-Based Solar Observatory (ASO-S/LST/WST) at 360 nm. *Solar Phys.* **299**, 11. DOI. ADS.

Karampelas, K., McLaughlin, J.A., Botha, G.J.J., Régnier, S.: 2022, Oscillatory reconnection of a 2D X-point in a hot coronal plasma. *Astrophys. J.* **925**, 195. DOI. ADS.

Kolotkov, D.Y., Nakariakov, V.M., Kupriyanova, E.G., Ratcliffe, H., Shibasaki, K.: 2015, Multi-mode quasi-periodic pulsations in a solar flare. *Astron. Astrophys.* **574**, A53. DOI. ADS.

Kontar, E.P., MacKinnon, A.L., Schwartz, R.A., Brown, J.C.: 2006, Compton backscattered and primary X-rays from solar flares: angle dependent Green's function correction for photospheric albedo. *Astron. Astrophys.* **446**, 1157. DOI. ADS.

Kou, Y., Cheng, X., Wang, Y., Yu, S., Chen, B., Kontar, E.P., Ding, M.: 2022, Microwave imaging of quasi-periodic pulsations at flare current sheet. *Nat. Commun.* **13**, 7680. DOI. ADS.

Krucker, S., Hurford, G.J., Grimm, O., Kögl, S., Gröbelbauer, H.-P., Etesi, L., Casadei, D., Csillaghy, A., Benz, A.O., Arnold, N.G., Molendini, F., Orleanski, P., Schori, D., Xiao, H., Kuhar, M., Hochmuth, N., Felix, S., Schramka, F., Marcin, S., Kobler, S., Iseli, L., Dreier, M., Wiehl, H.J., Kleint, L., Battaglia, M., Lastufka, E., Sathiapal, H., Lapadula, K., Bednarzik, M., Birrer, G., Stutz, S., Wild, C., Marone, F., Skup, K.R., Cichocki, A., Ber, K., Rutkowski, K., Bujwan, W., Juchnikowski, G., Winkler, M., Darmetko, M., Michalska, M., Seweryn, K., Białek, A., Osica, P., Sylwester, J., Kowalinski, M., Ścisłowski, D., Siarkowski, M., Stęślicki, M., Mrozek, T., Podgórski, P., Meuris, A., Limousin, O., Gevin, O., Le Mer, I., Brun, S., Strugarek, A., Vilmer, N., Musset, S., Maksimović, M., Fárník, F., Kozáček, Z., Kašparová, J., Mann, G., Önel, H., Warmuth, A., Rendtel, J., Anderson, J., Bauer, S., Dionies, F., Paschke, J., Plüschke, D., Woche, M., Schuller, F., Veronig, A.M., Dickson, E.C.M., Gallagher, P.T., Maloney, S.A., Bloomfield, D.S., Piana, M., Massone, A.M., Benvenuto, F., Massa, P., Schwartz, R.A., Dennis, B.R., van Beek, H.F., Rodríguez-Pacheco, J., Lin, R.P.: 2020, The spectrometer/telescope for imaging X-rays (STIX). *Astron. Astrophys.* **642**, A15. DOI. ADS.

Kupriyanova, E.G., Melnikov, V.F., Nakariakov, V.M., Shibasaki, K.: 2010, Types of microwave quasi-periodic pulsations in single flaring loops. *Solar Phys.* **267**, 329. DOI. ADS.
Kupriyanova, E., Kolotkov, D., Nakariakov, V., Kaufman, A.: 2020, Quasi-periodic pulsations in solar and stellar flares. Review. *Solar-Terr. Phys.* **6**, 3. DOI. ADS.
Lemen, J.R., Title, A.M., Akin, D.J., Boerner, P.F., Chou, C., Drake, J.F., Duncan, D.W., Edwards, C.G., Friedlaender, F.M., Heyman, G.F., Hurlburt, N.E., Katz, N.L., Kushner, G.D., Levay, M., Lindgren, R.W., Mathur, D.P., McFeaters, E.L., Mitchell, S., Rehse, R.A., Schrijver, C.J., Springer, L.A., Stern, R.A., Tarbell, T.D., Wuelser, J.-P., Wolfson, C.J., Yanari, C., Bookbinder, J.A., Cheimets, P.N., Caldwell, D., Deluca, E.E., Gates, R., Golub, L., Park, S., Podgorski, W.A., Bush, R.I., Scherrer, P.H., Gummin, M.A., Smith, P., Auker, G., Jerram, P., Pool, P., Soufli, R., Windt, D.L., Beardsley, S., Clapp, M., Lang, J., Waltham, N.: 2012, The Atmospheric Imaging Assembly (AIA) on the Solar Dynamics Observatory (SDO). *Solar Phys.* **275**, 17. DOI. ADS.
Li, D., Chen, W.: 2022, Quasi-periodic accelerations of energetic particles during a solar flare. *Astrophys. J. Lett.* **931**, L28. DOI. ADS.
Li, Y.P., Gan, W.Q.: 2008, Observational studies of the X-ray quasi-periodic oscillations of a solar flare. *Solar Phys.* **247**, 77. DOI. ADS.
Li, T., Zhang, J.: 2015, Quasi-periodic slipping magnetic reconnection during an X-class solar flare observed by the Solar Dynamics Observatory and Interface Region Imaging Spectrograph. *Astrophys. J. Lett.* **804**, L8. DOI. ADS.
Li, T., Yang, K., Hou, Y., Zhang, J.: 2016, Slipping magnetic reconnection of flux-rope structures as a precursor to an eruptive X-class solar flare. *Astrophys. J.* **830**, 152. DOI. ADS.
Li, D., Yuan, D., Su, Y.N., Zhang, Q.M., Su, W., Ning, Z.J.: 2018, Non-damping oscillations at flaring loops. *Astron. Astrophys.* **617**, A86. DOI. ADS.
Li, H., Chen, B., Feng, L., Li, Y., Huang, Y., Li, J.-W., Lu, L., Xue, J.-C., Ying, B.-L., Zhao, J., Yang, Y.-T., Gan, W.-Q., Fang, C., Song, K.-F., Wang, H., Guo, Q.-F., He, L.-P., Zhu, B., Zhu, C., Deng, L., Bao, H.-C., Cao, C.-X., Yang, Z.-G.: 2019, The Lyman-alpha Solar Telescope (LST) for the ASO-S mission — I. Scientific objectives and overview. *Res. Astron. Astrophys.* **19**, 158. DOI. ADS.
Li, B., Antolin, P., Guo, M.-Z., Kuznetsov, A.A., Pascoe, D.J., Van Doorsselaere, T., Vasheghani Farahani, S.: 2020, Magnetohydrodynamic fast sausage waves in the solar corona. *Space Sci. Rev.* **216**, 136. DOI. ADS.
Li, D., Shi, F., Zhao, H., Xiong, S., Song, L., Peng, W., Li, X., Chen, W., Ning, Z.: 2022, Flare quasi-periodic pulsation associated with recurrent jets. *Front. Astron. Space Sci.* **9**, 1032099. DOI. ADS.
Liang, B., Meng, Y., Feng, S., Yang, Y.: 2020, Estimating red noise in quasi-periodic signals with MCMC-based Bayesian. *Astrophys. Space Sci.* **365**, 40. DOI. ADS.
Lin, R.P., Schwartz, R.A.: 1987, High spectral resolution measurements of a solar flare hard X-ray burst. *Astrophys. J.* **312**, 462. DOI. ADS.
Lysenko, A.L., Ulanov, M.V., Kuznetsov, A.A., Fleishman, G.D., Frederiks, D.D., Kashapova, L.K., Sokolova, Z.Y., Svinkin, D.S., Tsvetkova, A.E.: 2022, KW-Sun: the konus-wind solar flare database in hard X-ray and soft gamma-ray ranges. *Astrophys. J. Suppl. Ser.* **262**, 32. DOI. ADS.
McLaughlin, J.A., Thurgood, J.O., MacTaggart, D.: 2012, On the periodicity of oscillatory reconnection. *Astron. Astrophys.* **548**, A98. DOI. ADS.
McLaughlin, J.A., Nakariakov, V.M., Dominique, M., Jelínek, P., Takasao, S.: 2018, Modelling quasi-periodic pulsations in solar and stellar flares. *Space Sci. Rev.* **214**, 45. DOI. ADS.
Meegan, C., Lichti, G., Bhat, P.N., Bissaldi, E., Briggs, M.S., Connaughton, V., Diehl, R., Fishman, G., Greiner, J., Hoover, A.S., van der Horst, A.J., von Kienlin, A., Kippen, R.M., Kouveliotou, C., McBreen, S., Paciesas, W.S., Preece, R., Steinle, H., Wallace, M.S., Wilson, R.B., Wilson-Hodge, C.: 2009, The Fermi gamma-ray burst monitor. *Astrophys. J.* **702**, 791. DOI. ADS.
Melnikov, V.F., Reznikova, V.E., Shibasaki, K., Nakariakov, V.M.: 2005, Spatially resolved microwave pulsations of a flare loop. *Astron. Astrophys.* **439**, 727. DOI. ADS.
Müller, D., St. Cyr, O.C., Zouganelis, I., Gilbert, H.R., Marsden, R., Nieves-Chinchilla, T., Antonucci, E., Auchère, F., Berghmans, D., Horbury, T.S., Howard, R.A., Krucker, S., Maksimovic, M., Owen, C.J., Rochus, P., Rodriguez-Pacheco, J., Romoli, M., Solanki, S.K., Bruno, R., Carlsson, M., Fludra, A., Harra, L., Hassler, D.M., Livi, S., Louarn, P., Peter, H., Schühle, U., Teriaca, L., del Toro Iniesta, J.C., Wimmer-Schweingruber, R.F., Marsch, E., Velli, M., De Groof, A., Walsh, A., Williams, D.: 2020, The Solar Orbiter mission. Science overview. *Astron. Astrophys.* **642**, A1. DOI. ADS.
Nakajima, H., Sekiguchi, H., Sawa, M., Kai, K., Kawashima, S.: 1985, The radiometer and polarimeters at 80, 35, and 17 GHz for solar observations at Nobeyama. *Publ. Astron. Soc. Japan* **37**, 163. ADS.
Nakariakov, V.M., Melnikov, V.F.: 2009, Quasi-periodic pulsations in solar flares. *Space Sci. Rev.* **149**, 119. DOI. ADS.
Nakariakov, V.M., Melnikov, V.F., Reznikova, V.E.: 2003, Global sausage modes of coronal loops. *Astron. Astrophys.* **412**, L7. DOI. ADS.

Nakariakov, V.M., Zimovets, I.V.: 2011, Slow magnetoacoustic waves in two-ribbon flares. *Astrophys. J. Lett.* **730**, L27. DOI. ADS.
Nakariakov, V.M., Foullon, C., Verwichte, E., Young, N.P.: 2006, Quasi-periodic modulation of solar and stellar flaring emission by magnetohydrodynamic oscillations in a nearby loop. *Astron. Astrophys.* **452**, 343. DOI. ADS.
Nakariakov, V.M., Anfinogentov, S.A., Antolin, P., Jain, R., Kolotkov, D.Y., Kupriyanova, E.G., Li, D., Magyar, N., Nisticò, G., Pascoe, D.J., Srivastava, A.K., Terradas, J., Vasheghani Farahani, S., Verth, G., Yuan, D., Zimovets, I.V.: 2021, Kink oscillations of coronal loops. *Space Sci. Rev.* **217**, 73. DOI. ADS.
Pesnell, W.D., Thompson, B.J., Chamberlin, P.C.: 2012, The Solar Dynamics Observatory (SDO). *Solar Phys.* **275**, 3. DOI. ADS.
Pugh, C.E., Broomhall, A.-M., Nakariakov, V.M.: 2017, Significance testing for quasi-periodic pulsations in solar and stellar flares. *Astron. Astrophys.* **602**, A47. DOI. ADS.
Reznikova, V.E., Shibasaki, K.: 2011, Flare quasi-periodic pulsations with growing periodicity. *Astron. Astrophys.* **525**, A112. DOI. ADS.
Shang, Z., Xu, K., Liu, Y., Wu, Z., Lu, G., Zhang, Y., Zhang, L., Su, Y., Chen, Y., Yan, F.: 2022, A broadband solar radio dynamic spectrometer working in the millimeter-wave band. *Astrophys. J. Suppl. Ser.* **258**, 25. DOI. ADS.
Shang, Z., Wu, Z., Liu, Y., Bai, Y., Lu, G., Zhang, Y., Zhang, L., Su, Y., Chen, Y., Yan, F.: 2023, The calibration of the 35-40 GHz solar radio spectrometer with the new Moon and a noise source. *Astrophys. J. Suppl. Ser.* **268**, 45. DOI. ADS.
Shi, F., Li, D., Ning, Z., Guo, Y., Feng, S., Xu, J.: 2023, Are quasi-periodic pulsations independent of loop oscillations in solar flare? *Astrophys. J.* **958**, 39. DOI. ADS.
Simões, P.J.A., Hudson, H.S., Fletcher, L.: 2015, Soft X-ray pulsations in solar flares. *Solar Phys.* **290**, 3625. DOI. ADS.
Simões, P.J.A., Reid, H.A.S., Milligan, R.O., Fletcher, L.: 2019, The spectral content of SDO/AIA 1600 and 1700 Å filters from flare and plage observations. *Astrophys. J.* **870**, 114. DOI. ADS.
Su, Y., Liu, W., Li, Y.-P., Zhang, Z., Hurford, G.J., Chen, W., Huang, Y., Li, Z.-T., Jiang, X.-K., Wang, H.-X., Xia, F.-X.-Y., Chen, C.-X., Yu, W.-H., Yu, F., Wu, J., Gan, W.-Q.: 2019, Simulations and software development for the Hard X-ray Imager onboard ASO-S. *Res. Astron. Astrophys.* **19**, 163. DOI. ADS.
Takasao, S., Shibata, K.: 2016, Above-the-loop-top oscillation and quasi-periodic coronal wave generation in solar flares. *Astrophys. J.* **823**, 150. DOI. ADS.
Thurgood, J.O., Pontin, D.I., McLaughlin, J.A.: 2017, Three-dimensional oscillatory magnetic reconnection. *Astrophys. J.* **844**, 2. DOI. ADS.
Thurgood, J.O., Pontin, D.I., McLaughlin, J.A.: 2019, On the periodicity of linear and nonlinear oscillatory reconnection. *Astron. Astrophys.* **621**, A106. DOI. ADS.
Tian, H., Young, P.R., Reeves, K.K., Wang, T., Antolin, P., Chen, B., He, J.: 2016, Global sausage oscillation of solar flare loops detected by the Interface Region Imaging Spectrograph. *Astrophys. J. Lett.* **823**, L16. DOI. ADS.
Torrence, C., Compo, G.P.: 1998, A practical guide to wavelet analysis. *Bull. Am. Meteorol. Soc.* **79**, 61. DOI. ADS.
Van Doorsselaere, T., Kupriyanova, E.G., Yuan, D.: 2016, Quasi-periodic pulsations in solar and stellar flares: an overview of recent results (invited review). *Solar Phys.* **291**, 3143. DOI. ADS.
Van Doorsselaere, T., De Groof, A., Zender, J., Berghmans, D., Goossens, M.: 2011, LYRA observations of two oscillation modes in a single flare. *Astrophys. J.* **740**, 90. DOI. ADS.
Vaughan, S.: 2005, A simple test for periodic signals in red noise. *Astron. Astrophys.* **431**, 391. DOI. ADS.
Vaughan, S.: 2010, A Bayesian test for periodic signals in red noise. *Mon. Not. Roy. Astron. Soc.* **402**, 307. DOI. ADS.
Wang, T.J., Solanki, S.K., Innes, D.E., Curdt, W., Marsch, E.: 2003, Slow-mode standing waves observed by SUMER in hot coronal loops. *Astron. Astrophys.* **402**, L17. DOI. ADS.
Wang, T., Ofman, L., Yuan, D., Reale, F., Kolotkov, D.Y., Srivastava, A.K.: 2021, Slow-mode magnetoacoustic waves in coronal loops. *Space Sci. Rev.* **217**, 34. DOI. ADS.
Yan, F., Wu, Z., Shang, Z., Wang, B., Zhang, L., Chen, Y.: 2023, The first flare observation with a new solar microwave spectrometer working in 35 – 40 GHz. *Astrophys. J. Lett.* **942**, L11. DOI. ADS.
Yuan, D., Van Doorsselaere, T.: 2016a, Forward modeling of standing kink modes in coronal loops. I. Synthetic views. *Astrophys. J. Suppl. Ser.* **223**, 23. DOI. ADS.
Yuan, D., Van Doorsselaere, T.: 2016b, Forward modeling of standing kink modes in coronal loops. II. Applications. *Astrophys. J. Suppl. Ser.* **223**, 24. DOI. ADS.
Yuan, D., Feng, S., Li, D., Ning, Z., Tan, B.: 2019, A compact source for quasi-periodic pulsation in an M-class solar flare. *Astrophys. J. Lett.* **886**, L25. DOI. ADS.
Zhang, Z., Chen, D.-Y., Wu, J., Chang, J., Hu, Y.-M., Su, Y., Zhang, Y., Wang, J.-P., Liang, Y.-M., Ma, T., Guo, J.-H., Cai, M.-S., Zhang, Y.-Q., Huang, Y.-Y., Peng, X.-Y., Tang, Z.-B., Zhao, X., Zhou, H.-H.,

Wang, L.-G., Song, J.-X., Ma, M., Xu, G.-Z., Yang, J.-F., Lu, D., He, Y.-H., Tao, J.-Y., Ma, X.-L., Lv, B.-G., Bai, Y.-P., Cao, C.-X., Huang, Y., Gan, W.-Q.: 2019, Hard X-ray Imager (HXI) onboard the ASO-S mission. *Res. Astron. Astrophys.* **19**, 160. DOI. ADS.

Zimovets, I.V., Kuznetsov, S.A., Struminsky, A.B.: 2013, Fine structure of the sources of quasi-periodic pulsations in "single-loop" solar flares. *Astron. Lett.* **39**, 267. DOI. ADS.

Zimovets, I.V., McLaughlin, J.A., Srivastava, A.K., Kolotkov, D.Y., Kuznetsov, A.A., Kupriyanova, E.G., Cho, I.-H., Inglis, A.R., Reale, F., Pascoe, D.J., Tian, H., Yuan, D., Li, D., Zhang, Q.M.: 2021, Quasi-periodic pulsations in solar and stellar flares: a review of underpinning physical mechanisms and their predicted observational signatures. *Space Sci. Rev.* **217**, 66. DOI. ADS.